# 25

# Dynamic Modeling and Performance Trade-offs in Flexure-based Positioning and Alignment Systems[1]

Vijay Shilpiekandula and Kamal Youcef-Toumi
*Mechatronics Research Laboratory, Department of Mechanical Engineering*
*Massachusetts Institute of Technology, Cambridge, MA 02139,*
*USA*

## 1. Introduction

Precision positioning and alignment are critical to an emerging class of small-scale manufacturing and numerous motion control applications. The drive for better performance steers design and control effort into achieving high tolerances and stringent specifications in terms of parameters, such as resolution, range, load-capacity, and bandwidth. Examples of applications needing precision positioning and alignment include (i) high-bandwidth steering of mirrors in telecommunication applications [1], (ii) tool-sample alignment in stamping applications such as imprint lithography [2, 3] and micro-contact printing [4], and (iii) alignment of optically flat surfaces brought in close proximity to characterize fields and forces on small-scales, such as the Casimir force [5, 6].

A widely used set of designs for precision applications described above involve compliant mechanisms based on slender beam modules, also referred to as flexures [7, 8]. The advantages flexures offer are mainly smooth elastic motion without non-linearities such as friction or backlash [9]. Flexure-based mechanisms such as the diaphragm flexure involve the payload suspended on a radial or tangential arrangement of flexural beams. Various forms of such flexures have appeared over the past few decades for applications such as MEMS mirrors, and in angle alignment and guidance applications [4, 10, 11]. Analysis of the statics and dynamics of flexure-based mechanisms have been extensively studied [9, 12].

While flexure-based engineering designs have been around for many decades [13], designing them for dynamic performance has sought little attention. Few publications [14, 15] have appeared in this context. The design for dynamical performance of flexures in the context of mechanical advantage is detailed in [14]. A finite-element approach based on Euler-Bernoulli beam bending theory is formulated for analyzing dynamics in [15] and optimizing the design space for precision flexure-based applications in [16].

---



Source: Motion Control, Book edited by: Federico Casolo,
ISBN 978-953-7619-55-8, pp. 580, January 2010, INTECH, Croatia, downloaded from SCIYO.COM

We build on the work presented in the literature and integrate models that can enhance the accuracy in predicting the dynamics of a given flexure-based design by including the effects of distributed mass and compliance of the flexures covering shear and rotational effects. These effects are shown to dominate at small flexure lengths. Further, we use the models to characterize design space parameters such as range, load-capacity, and bandwidth. While most of the current literature in flexure-based designs focuses on static values of performance variables such as angular position, or acceleration, we present a state-space approach for characterizing the bounds on these variables in the frequency domain. This is critical for ensuring that performance requirements are met within the usually large bandwidths of operation, an example application being fast steering of mirrors in telecommunications [1].

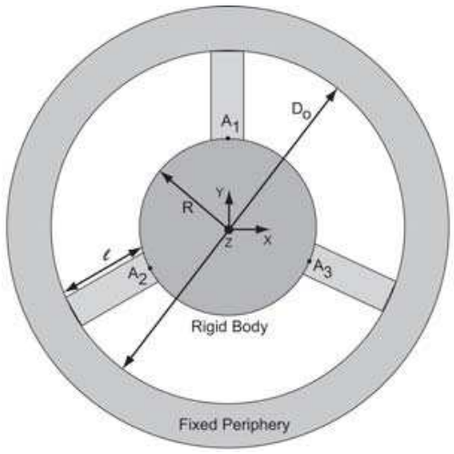


Fig. 1. A diaphragm flexure as a parallel kinematic mechanism with a central rigid mass connected by $n$ = 3 flexural beam units to the ground. The dimension $D_0 = 2\ell + 2R$ is referred in this chapter as the footprint of the mechanism. The **Z** axis is shown pointing out of the page.

This chapter is organized as follows. In Section 2 we assemble lumped parameter models for a diaphragm flexure design. Section 3 covers the closed-form characterization of the design space from the dynamic models. Non-dimensional design plots and the efficacy of the models in capturing shear effects at small flexure lengths are addressed in this section. A state-space approach is used for characterizing key performance variables in Section 4. This section taps into multi-input multi-output (MIMO) analysis tools to develop a framework for mapping design requirements over to the state-space. The effects of manufacturing errors are studied in the context of decoupling and asymmetry in this section. Finally, we conclude with a summary of the contributions of the work.

## 2. Dynamic modeling

Our goal is to capture the out-of-plane behavior, i.e. the vertical translation, pitch, and roll degrees of freedom of diaphragm flexures used in precision angle alignment mechanisms. In this section, we assemble dynamic models for a class of diaphragm flexures – namely, those applying radial constraints on a central rigid mass via flexural beam units. We derive lumped parameter models representing the mass and stiffness of the diaphragm flexure. The applications of compliant mechanisms using the simple flexural beam units studied

here span multiple scales from MEMS to meso-scale systems. In all these applications, it is desirable to develop accurate models since the mechanisms constitute the plant in the overall closed-loop control system.

### 2.1 Modeling flexural beam

To model bending of the flexural beam unit, shown in Fig. 2, we use a Timoshenko beam [17] model since a simple Euler-Bernoulli beam model cannot capture the effects of shear and rotational inertia. As will be shown later, these effects become significant for short beams, which are widely used in compliant mechanisms spanning multiple length scales. To model torsion of the flexural element, we use St. Venant's torsion formulation assuming that (i) the effects of restrained warping are negligible and (ii) bending and torsion are decoupled. Further, we assume that the deflections of the flexural beam element are small (an order of magnitude smaller than the beam thickness) and hence, neglect the effects of axial stretching and the resultant stress stiffening along the length of the beam element.

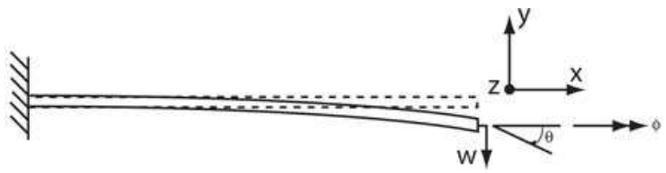


Fig. 2. Schematic diagram showing a flexural beam element with deflection $\omega(x,\ t)$, slope $\theta(x,\ t)$, and twist about the X-axis by an angle $\phi(x,\ t)$.

Under the above-mentioned assumptions, the distributed parameter model for the beam is well-documented in the literature [17] as being depicted by a set of partial differential equations in the deflection $w(x,\ t)$, slope $\theta(x,\ t)$, and angle of twist $\phi(x,\ t)$ listed in Section **A. 1** of the Appendix.

The infinite-dimensional behavior governed by the set of partial differential equations can be approximated to that arising for a one-element model using the method of assumed modes [18]. By this method, the infinite-dimensional behavior of the mechanism is approximated to a finite-series made up of spatially varying mode shape functions (or trial functions) with temporally varying mode amplitudes [19]. Since a one-element model is used for the beam, the distributed properties of the beam are lumped to the node at the guided end of the beam; the fixed node of the beam has no lumped mass or stiffness. Hence, from the three displacements assumed for the guided end of the beam, a three-DOF lumped parameter model can be derived.[2]

The detailed application of the assumed modes method to the set of partial differential equations governing the motion of the Timoshenko beam can be found in parts in [20] and [21]. The key results used in this work are highlighted here. Under the geometric boundary conditions of (i) one end $x$ = 0 of the flexural beam being grounded and (ii) the other end $x = \ell$ subject to generalized displacements $\mathbf{V}(t) = [w(\ell,\ t)\ \theta(\ell,\ t)\ \phi(\ell,\ t)]^T$, (where $w(\ell,\ t)$ is the vertical deflection, $\theta(\ell,\ t)$ the slope, and $\phi(\ell,\ t)$ is the angle of twist), the corresponding 3×3 matrices – mass $\mathbf{M}_f$ and stiffness $\mathbf{K}_f$ are as given below:

[2] A many-element model can be used for each flexural beam to develop higher-order lumped parameter models, if desired.

$$\mathbf{M}_f = \begin{bmatrix} M_1 & M_2 & 0 \\ M_2 & M_3 & 0 \\ 0 & 0 & M_4 \end{bmatrix}; \quad \mathbf{K}_f = \begin{bmatrix} K_1 & K_2 & 0 \\ K_2 & K_3 & 0 \\ 0 & 0 & K_4 \end{bmatrix} \tag{1}$$

where the matrix values depend on material properties and geometry, and are tabulated in Section **A. 1** of the Appendix. Zeroes in either matrix result from the decoupling assumed between bending and torsion. The lumped mass and stiffness matrices are used as building blocks for assembling dynamic models of mechanisms involving flexural beam units. Note that we need to restrict these matrix building blocks to parallel kinematic configurations since the geometric boundary conditions corresponding to $x$ = 0 have been assumed to be all zero. Formulations for serial kinematic configurations can be developed by altering this set of geometric boundary conditions [20].

### 2.2 Assembling global lumped parameter model

Here, we formulate the dynamics of parallel kinematic mechanisms that contain a rigid body connected to the ground through a multitude of flexural beam units. We integrate the lumped parameter model for the flexural beam in Section 2 with rigid body dynamical models using appropriate transformations to obtain the global model [15]. These transformations are chosen to ensure the continuity of nodal displacements at the interface between the rigid body and the flexures.

Consider a parallel kinematic mechanism with a central rigid circular disk centered at the origin and parallel to the horizontal **XY** plane of the cartesian **XYZ** space, as shown in Fig. 1. In the rest position, the principal axes of the disk **X**', **Y**', and **Z**' coincide with the cartesians axes **X**, **Y**, and **Z**, respectively. Let the disk be of radius $R$, thickness $T$, mass $M_R$, and moments of inertia $J_{Rxx}$ and $J_{Ryy}$ about the X and Y axes respectively. A number $n$ of slender beam flexures, each of width $W$, thickness $H$, and length $\ell$, are in the **XY** plane connecting every peripheral point $P_i$ to the ground. The coordinates of $P_i$ in the **X**'**Y**' plane are ($Rcos\alpha_I$,$Rsin\alpha_i$) with angles $\alpha_i \in$[0, 2$\pi$) for $i$ = 1, 2, 3… $n$.

Since the beams provide high axial (and hence in-plane **XY**) stiffness and low out-of-plane stiffness, we expect that the dominant modes correspond to the out-of-plane motion, namely vertical deflection, pitch, and roll. We hence assume that the out-of-plane motion of the disk is decoupled from the in-plane motion, i.e. the center of the disk always moves only vertically. For small vertical deflection $z(t)$ of the center of mass, and small angular rotations $\theta_x(t)$ and $\theta_y(t)$ about the **X** and **Y** axes respectively, the principal plane **X**'**Y**' of the disk moves out of the **XY** plane to the one depicted by

$$\mathbf{Z}_p(t) = \theta_y(t)\mathbf{X} + \theta_x(t)\mathbf{Y} + z(t) \tag{2}$$

For continuity of displacement at each of the nodes $P_i$, Eq. (2) can be used to show that the end-displacements $\mathbf{V}_i(t)$ of every $i^{th}$ flexure are related to the global generalized (rigid body) displacements $\mathbf{V}_R(t)$ as follows:

$$\mathbf{V}_i(t) = \begin{Bmatrix} w_i(\ell,t) \\ \theta_i(\ell,t) \\ \phi_i(\ell,t) \end{Bmatrix} = \Re \begin{Bmatrix} z(t) \\ \theta_x(t) \\ \theta_y(t) \end{Bmatrix} = \Re \mathbf{V}_R(t) \tag{3}$$

where the transformation matrix $\Re$=

$$\begin{bmatrix} 1 & Rsin\alpha_i & Rcos\alpha_i \\ 0 & -sin\alpha_i & -cos\alpha_i \\ 0 & -cos\alpha_i & -sin\alpha_i \end{bmatrix} \quad (4)$$

### 2.3 Dynamics

Based on the mass and stiffness properties of the individual flexural beam units connected to the central rigid body, we need to derive the mass **M** and stiffness **K** properties of the assembly.

By formulating the Lagrangian of the assembly in terms of the rigid body displacements $\mathbf{V}_R(t)$, we develop the lumped mass and stiffness matrices of the overall parallel kinematic mechanism as follows:

$$\mathbf{M} = \sum_{i=1}^{n} \Re^T \mathbf{M}_{fi} \Re + \mathbf{M}_R; \ \mathbf{K} = \sum_{i=1}^{n} \Re^T \mathbf{K}_{fi} \Re \quad (5)$$

where$\mathbf{M}_{fi}$ and $\mathbf{K}_{fi}$ are the lumped mass and stiffness matrices, respectively, of the individual flexure building blocks given in Section 2.1, and Tables 4 and 5; $\mathbf{M}_R$ is the mass matrix of the rigid body and is given by:

$$\begin{bmatrix} M & 0 & 0 \\ 0 & J_{Rxx} & 0 \\ 0 & 0 & J_{Ryy} \end{bmatrix} \quad (6)$$

The equations of motion of the lumped parameter representation, for the free response case, is in the form given below:

$$\mathbf{M}\ddot{\mathbf{V}}_R + \mathbf{B}\dot{\mathbf{V}}_R + \mathbf{K}\mathbf{V}_R = \mathbf{0} \quad (7)$$

Note that we have not presented the modeling of damping matrix **B** in this chapter. Models such as proportional damping, given by $\mathbf{B} = b_m\mathbf{M}+b_k\mathbf{K}$, are widely used in the literature [22], where $b_m$ and $b_k$ are constants that depend on material properties and are experimentally determined from sine-sweep frequency response measurements. For the design of active or passive damping in flexure mechanisms, a survey and foam-based methods are detailed in [23].

## 3. Dynamic performance of diaphragm flexures

In this section, we use the dynamic models developed from Section 2.3 to examine (i) the influence of geometric arrangement of flexures on coupling between the global generalized displacements or modes, (ii) the best bandwidth possible for a given foot-print of a symmetric diaphragm flexure mechanism, and (iii) the performance trade-offs between parameters such as range, bandwidth, and load-capacity for the same.

### 3.1 Coupling

From the equations of motion of the diaphragm flexure derived in Section 2.3, the geometrical layout of flexural constraints that allow for static and dynamic decoupling of

the three DOFs can be determined. For static decoupling, the off-diagonal terms in the overall stiffness matrix **K** should be zero. For dynamic decoupling, the off-diagonal terms in both the mass **M** and stiffness **K** matrices should be zero.

Static and dynamic decoupling is desirable, for instance, when the diaphragm flexure mechanism is controlled to vertically position the central rigid mass while ensuring low error motions in the other DOFs, namely pitch and roll. Stable decoupled systems tend to be more amenable to low error motions even under open-loop control. It should, however, be noted that perfect decoupling cannot be achieved in practice owing to non-uniformities arising from manufacturing or material properties. Nonetheless, designing a compliant mechanism to be as close to a decoupled dynamic system as possible is desirable [24]. Here, we examine conditions under which such decoupling is possible for a diaphragm flexure mechanism.

Substituting the values of $\Re$ from Eq. (4) into Eqs. (5) and (5), and given Eqs. (1) and (6), the conditions necessary for the off-diagonal terms in the global mass **M** and stiffness **K** matrices to be zero are as follows:

$$\sum_{i=1}^{n} cos\alpha_i = 0; \quad \sum_{i=1}^{n} sin\alpha_i = 0; \quad \sum_{i=1}^{n} sin2\alpha_i = 0; \tag{8}$$

Hence, the geometric arrangement of a number $n \geq 3$ of flexures around the central rigid mass allows for the overall mechanism to be close to being statically and dynamically decoupled if the above conditions are satisfied. Note here that each individual flexure of the mechanism has its vertical deflection and slope coupled (both statically and dynamically), it is only the parallel combination of three or more of them that allow for the decoupling between the global modes to occur. Some possible design layouts that satisfy Eq. (8) are discussed in Section **A. 2** of the appendix. The effect of deviations from perfect symmetry on design requirements such as maximum deflection, velocity, and acceleration are studied in Section 4.

### 3.2 Natural frequencies

The best –3 $dB$ bandwidth possible for a closed-loop system depends on many factors, including the natural frequencies or poles of the open-loop plant. Fig. 3 shows the plots of undamped natural frequencies of the first three modes of the symmetric diaphragm flexure of Fig. 1. The plots show the variation corresponding to diaphragm flexure configurations with flexural beam length, $\ell$, varied in the range of about 0.5 $in$ to 3 $in$, while keeping the footprint $2\ell$+$2R$ at a constant value of 7 $in$. This constant footprint is chosen as a scaling factor for the length dimension and will be used in Section 3.3 to normalize all lengths in the design to formulate a non-dimensional study.

The plots of Fig. 1 show values of the undamped natural frequencies obtained from models based on St. Venant's torsion theory and one of two distinct beam bending theories – either (i) Timoshenko beam bending theory, or (ii) Euler Bernoulli beam bending theory. As explained earlier, the former beam bending theory accounts for shear and rotational effects versus, while the latter does not. In the plots of the figure, the frequency values obtained from a commercial FEA package are superimposed for comparison of the chosen models.

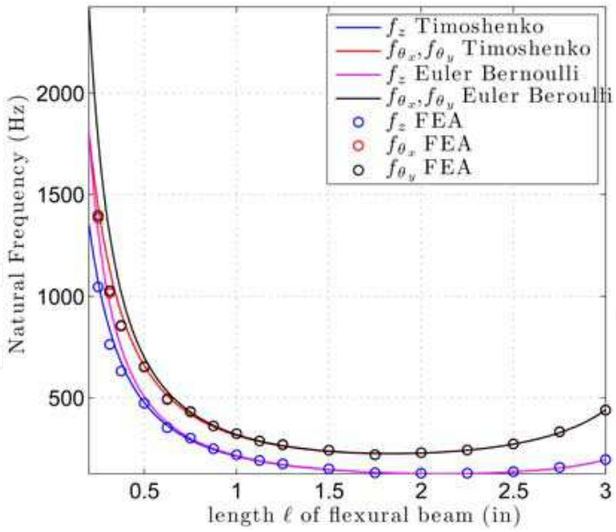


Fig. 3. Plot of undamped natural frequencies of first three modes of the symmetric diaphragm flexure of Fig. 1 for flexure beam length $\ell$ varying from about 0.2 $in$ to 3 $in$, keeping footprint $D_0 = 2\ell+2R$ at a constant value of 7$in$. Other parameter values used in the simulation are: beam width $W$ = 0.75 $in$, beam thickness $H$ = 0.1 $in$, central rigid disk thickness $T$ = 2.5 $in$, poisson's ratio $\nu$ = 0.33, elastic modulus $E$ = 69 $GPa$, density $\rho$ = 2700 $\frac{kg}{m^3}$.

The trends observed for the variation of natural frequencies for small flexural beam lengths is as expected, since small beam lengths result in large stiffness. Since the footprint is maintained constant, smaller beam lengths also imply large radius of the central disk and hence larger moving mass. However, the cubic dependence of stiffness on beam length dominates over the square dependence of mass on radius of the disk; hence the large natural frequencies at short beam lengths. For large beam lengths, the radius of the central disk is small, and hence the moving mass.[3] This effect is marginally larger than the loss in stiffness and hence the slight increase in natural frequency at large beam lengths.

For flexural beam lengths smaller than the shear approximation length factor $c \approx 0.6$ $in$, the Timoshenko model matches the trend from the FEA data better than the Euler-Bernoulli model. This confrms the prediction that shear effects dominate at small beam lengths and agrees with similar observations supporting the Timoshenko beam bending models for depicting the natural frequencies of short AFM cantilevers in [25].

Closed-form expressions for the natural frequency of the first three-dominant modes in the decoupled case, for large flexure lengths, are presented in Table 1. These expressions can be used as part of formulating an optimization problem, or to gain useful insights from parametric dependencies in designing a precision angular alignment setup based on diaphragm flexures.

[3] At the length scale of the diaphragm flexure discussed here, the moving mass is mainly composed of the central rigid disk. The lumped mass of the flexural beam is small at this length scale. However, it can be higher in other length scales, as in the case of a torsional MEMS mirror.

$$\omega_z = \sqrt{\frac{\frac{3EWH^3}{L^3}}{m+\frac{39}{35}m_f}}$$

$$\omega_{\theta_x,\theta_y} = \sqrt{\frac{\frac{3EWH^3}{L^3}(L^2+3R^2+3LR)+\frac{GWH^3}{2L^3}}{m(\frac{3R^2+T^2}{12})+m_f(\frac{L^2+39R^2+11LR}{70}+\frac{W^2+H^2}{24})}}$$

Table 1. Closed-form expressions for natural frequencies of first three modes of diaphragm flexure.

### 3.3 Performance trade-offs

The design space for utilizing flexure-based precision angular alignment mechanisms can be characterizing in terms of key parameters such as the range, payload capacity, and bandwidth. Fig. 4 shows the variation of the key non-dimensionalized performance parameters as a function of the non-dimensional flexural beam length $\ell$ for all diaphragm flexures with a constant footprint of $D = 2\ell + 2R$. The performance parameters plotted in the figure are (i) the natural frequencies of the first three modes, namely deflection $z$ and the two rotations $\theta_x$ and $\theta_y$, (ii) the maximum load-capacity, $F_{max}$, defined as the load that causes the resultant axial stress in the flexural beams to reach the yield strength, $\sigma_Y$, of the material within a safety factor $\eta$, and (iii) the maximum vertical deflection $\delta_{max}$, i.e. range under a given load. The normalization factors used for non-dimensionalizing the parameters are tabulated in Table 3, where $\rho$ and $E$ are the density and elastic modulus, respectively, of the material constituting the diaphragm flexure $\sigma$.

| $\sigma$ | $F_{max}$ | $K$ |
|---|---|---|
| $6\frac{Fl}{bh^2}$ | $\frac{3EI}{l^3}$ | $\frac{1}{6}\sigma_{max}\frac{bh^2}{l}$ |
| $\frac{3}{2}\frac{Fl}{bh^2}$ | $\frac{24EI}{l^3}$ | $\frac{2}{3}\sigma_{max}\frac{bh^2}{l}$ |
| $\frac{3}{2}\frac{Fl}{bh^2}$ | $\frac{12EI}{l^3}$ | $\frac{2}{3}\sigma_{max}\frac{bh^2}{l}$ |

Table 2. Flexural Building blocks Comparison

| Parameter | Normalization Factor |
|---|---|
| $\ell$ | $D = 2\ell + 2R$ |
| $f_z, f_{\theta_x}, f_{\theta_y}$ | $f_0 = \frac{1}{4\pi}\sqrt{\frac{E}{\rho D^2}}$ |
| $F_{max}$ | $F_0 = \frac{1}{6}\frac{WH^2}{D}\frac{100\sigma_Y}{\eta}$ |
| $\delta_{max}$ | $\delta_0 = \frac{10^6 F_0}{ED}$ |

Table 3. Normalization factors used for Design Parameters in Fig. 4.

The trade-off between load-capacity and range at different flexural beam lengths is evident from the figure. Small beam lengths allow for large load capacity and low range, whereas large beam lengths allow for low load capacity and large range. Natural frequencies are relatively low for intermediate beam lengths. The trade-off between natural frequencies and range is evident for small beam lengths, since stiffer beams have smaller deflections. The compromise between natural frequency and range is relatively mild at large beam lengths. An extension of the dynamic performance tradeoff characterization to the case of $n = 6$ flexural beams is presented in Fig. 5. From kinematic exact-contraint theory, it is known that only three constraints are needed to curb the three in-plane degrees of freedom of the rigid body. Thus for the case $n = 6$, three of the remaining constraints are redundant.

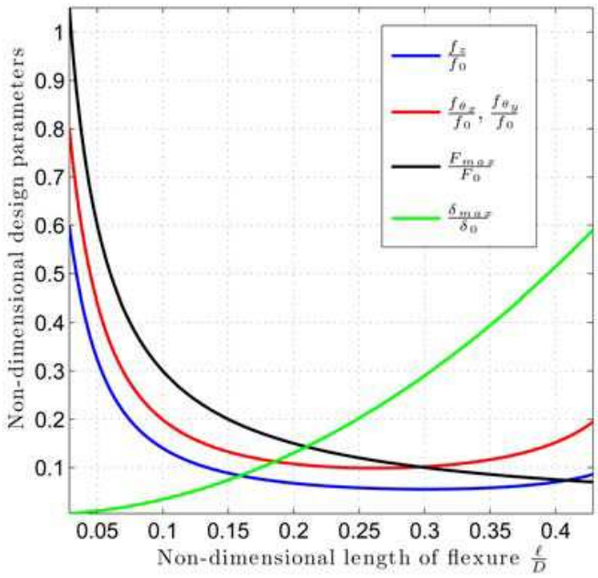


Fig. 4. Non-dimensional plots capturing the key dynamic performance parameters for diaphragm flexures of Fig. 3 with $n$ = 3 flexural beams of the same footprint D, but different flexure lengths ranging in the approximate range 0-0.45 D. The parameters of interest are (i) the natural frequency of first three modes $f_z$, $f_{\theta_x}$, and $f_{\theta_y}$, all normalized by $f_0$, (ii) load capacity $F_{max}$ normalized by $F_0$ and (iii) static vertical range $\delta_{max}$ normalized by $\delta_0$.

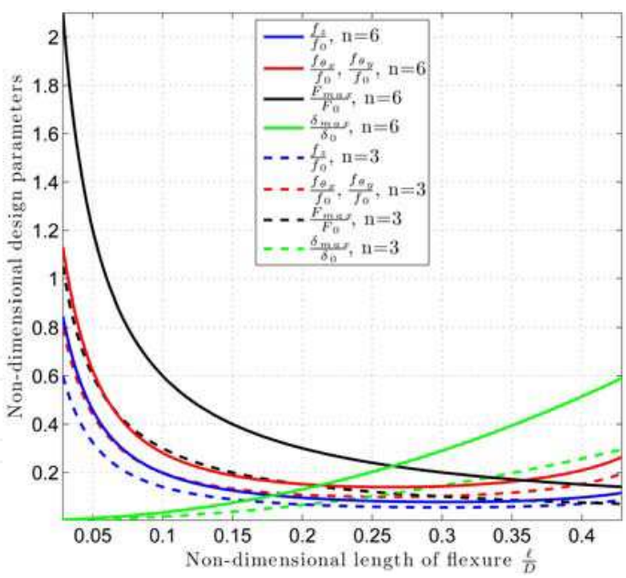


Fig. 5. Design parameter variations (shown as solid lines) captured for the case of double the number of flexures, i.e. $n$ = 6, as compared to the case of $n$ = 3 (shown as dashed lines) captured in Fig. 4.

The redundancy comes with added features which are desirable and facilitate improving the performance as follows. Since the load is distributed between larger number of flexures, the load-capacity envelope in this case is pushed higher to double that of the $n$ = 3 case. The

stiffnesses sum up since the flexural beams are arranged in a parallel combination. The resultant range is hence unchanged from that of the case of $n$ = 3. The added slight benefit is that there is no reduction in the natural frequencies. Instead, there is an almost $\sqrt{2}$ increase in the natural frequency of all the first three modes. This increase can be explained from the doubling of stiffness and constancy of mass, since the added mass of the flexures is small compared to the rigid body here. Therefore, increasing the number of flexural beams offers improved performance in terms of range, load-capacity, and natural frequencies.

## 4. State-space performance analysis

Characterization of parameters such as maximum displacement (or range), maximum velocity and acceleration is critical for precision motion control applications. A procedure for identifying the static ($\omega$ = 0) values of these parameters is developed for precision control of ball-screw drives in [26]. In this section, we present a state-space approach for determining the design performance parameters – maximum values of deflection (or range), velocity, and acceleration that are possible not only for static ($\omega$ = 0) but for a large range of operating frequencies.

We follow the approach for the case of a diaphragm flexure used for precision angle alignment. To account for the case when symmetry cannot be ensured for the diaphragm flexure, we assume a coupled multi-input multi-output (MIMO) model, as against a collection of independent single-input single-output (SISO) models. We focus our analyses to parameters such as maximum vertical and angular displacement (range), velocity, and acceleration. The presented approach can be extended to map other design parameters to the state-space. Further, while the ideas presented here are general and applicable to the case when state or output feedback control is used as well, we focus our analysis on just the open-loop system.

### 4.1 State space formulation

We begin with a state vector **x** containing the generalized coordinates depicting the equations of motion of the system. One choice of state variables could be the generalized displacements and their first-order derivatives.

$$\dot{\mathbf{x}}_{m\times 1} = \mathbf{A}_{m\times m}\mathbf{x}_{m\times 1} + \mathbf{B}_{m\times r}\mathbf{u}_{r\times 1} \tag{9}$$

$$\mathbf{y}_{p\times 1} = \mathbf{C}_{p\times m}\mathbf{x}_{m\times 1} + \mathbf{D}_{p\times r}\mathbf{u}_{r\times 1} \tag{10}$$

The goal here is to find the maximum values of displacements, velocities, and acceleration for any set of inputs (which can be oriented in any direction in the input space). That means we need to compute the upper bounds on the amplification of a scalar component $x_i$, which is derived as:

$$x_i = \mathbf{E}_{i\,1\times m}\mathbf{x}_{m\times 1} \tag{11}$$

where the $i^{th}$ element of the row vector $\mathbf{E}_i$ is 1 and the rest of the $m$ – 1 elements are zero. The component $x_i$ can be any design variable, such as angular velocity, or vertical deflection of the diaphragm flexure.

For a chosen control law, in the Laplace domain, the following relations hold between the state vector $\mathbf{X}(s)_{m\times 1}$, its $i^{th}$ component $X_i(s)$, and the input vector $\mathbf{U}(s)$:

$$\mathbf{X}(s)_{m\times 1} = \mathbf{G}(s)_{m\times r}\mathbf{U}(s)_{r\times 1} \tag{12}$$

$$X_i(s)_{1\times 1} = \mathbf{E}_{i1\times m}\mathbf{G}(s)_{m\times r}\mathbf{U}(s)_{r\times 1} \tag{13}$$

The maximum amplification [27] of the component $X_i(s)$ for a given input $\mathbf{U}(s)$ can be expressed as the 2-induced (Euclidean) norm of the gain matrix $\mathbf{E}_{i1\times m}\mathbf{G}(s)_{m\times r}$. For the choice of $\mathbf{E}_i$, the gain matrix reduces to the $i^{th}$ row of $\mathbf{G}(s)$. Hence, its 2-induced norm reduces to a vector norm, and is given by its lone singular value. This singular value of $\mathbf{E}_{i1\times m}\mathbf{G}(s)_{m\times r}$ is always smaller than or equal to the singular values of the matrix $\mathbf{G}(s)$ and hence provides a tighter bound on the amplification of $X_i(s)$.

### 4.2 Application to diaphragm flexure

We now apply the above formulation to the case of the diaphragm flexure of Fig. 3 to derive tight upper bounds[4] on the amplification of state vector components, such as vertical deflection, or say, maximum angular velocity of the diaphragm flexure in a given control situation. We do not consider the feedback control problem here; however, the proposed method can be extended to that case as well.

The state vector $\mathbf{x}(t)$ and the input vector $\mathbf{u}(t)$ for a configuration with three linear actuators pushing down on the central rigid body at three locations $Q_i(Rcos\beta_I, Rsin\beta_i)$, for $i$ = 1, 2, 3, are given as:

$$\mathbf{x}(t) = \begin{bmatrix} z(t) \\ \dot{z}(t) \\ \theta_x(t) \\ \dot{\theta}_x(t) \\ \theta_y(t) \\ \dot{\theta}_y(t) \end{bmatrix}; \quad \mathbf{u}(t) = \begin{bmatrix} F_1(t) \\ F_2(t) \\ F_3(t) \end{bmatrix}$$

The matrix $\mathbf{A}$ is assembled from components of $\mathbf{M}^{-1}\mathbf{K}$ from Eq. (5), and accounting for the derivative relationship pairs between the components of the state vector. By determining the force and moment components, the matrix $\mathbf{B}$ is given as

$$\begin{bmatrix} 0 & 0 & 0 \\ 1 & 1 & 1 \\ 0 & 0 & 0 \\ Rcos\beta_1 & Rcos\beta_2 & Rcos\beta_3 \\ 0 & 0 & 0 \\ -Rsin\beta_1 & -Rsin\beta_2 & -Rsin\beta_3 \end{bmatrix}$$

With the choice of $\mathbf{E}_i$ as described earlier, the maximum bound on each of the components of the state vector are found as shown in Fig. 6 for the diaphragm flexure of Fig. 3 containing three flexural beam units arranged symmetrically around the central rigid mass, and with

[4] The lower bound is zero, since for zero inputs, the components of the state vector are all zero.

linear actuators located at angles, $\beta_1 = 0$, $\beta_2 = \frac{2\pi}{3}$, $\beta_3 = \frac{4\pi}{3}$. The system is decoupled as seen from the variation of the singular values. With zero damping at the resonance peak, the maximum values of all variables assume exceedingly large values at the resonance frequency.

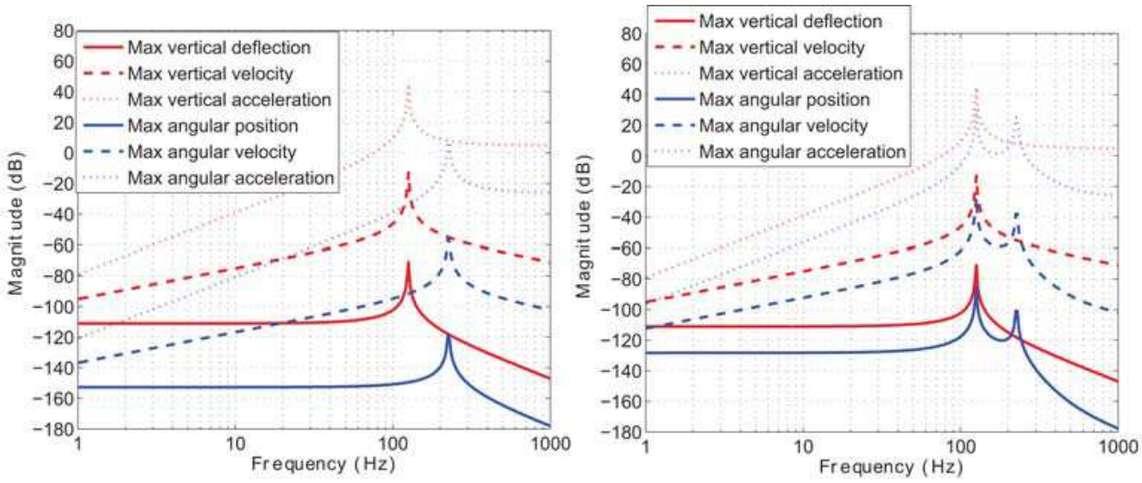


Fig. 6. The maximum amplification of states for an unit input vector (along any direction in the position space) is plotted for the case of three flexural beam units arranged symmetrically around the central rigid mass.

### 4.3 Effect of deviation from symmetry

The same analysis is repeated for the case when a 1° misalignment of one of the flexural beam units is caused by a manufacturing error. The system is now coupled, with deflection and angular position being dependent on each other, as seen from the two resonance peaks appearing in the variation of the singular values. This coupling implies that the angular position can assume exceedingly large values at a resonance frequency lower than that expected when perfect symmetry is ensured. The input directions that correspond to the maximum bound on a component $X_i(j\omega)$ at a chosen frequency $\omega$ lie along the right eigen vectors of the matrix $\mathbf{G}_i(j\omega)\mathbf{G}_i^H(j\omega)$, where $\mathbf{G}_i(j\omega)$ is the $i^{th}$ row of the matrix $\mathbf{G}(j\omega)$.

In summary, the benefits of using this approach for specifying the design performance variables are two fold – (i) it is applicable in case of deviations from perfect symmetry, allowing to analyze the effects of the deviations, and (ii) it gives the bounds not only for the static case ($\omega$= 0) but also for the desired frequency range of interest. This approach can be incorporated into the design decision-making process, along with other important considerations, such as constraints imposed by physical limits, for example, saturation of the actuators, or limit stops in the path of a motion stage.

## 5. Conclusions

We have examined the need for diaphragm flexures in precision angular positioning applications. To accurately characterize the dynamics, we assembled lumped parameter models from mass and stiffness matrices for individual flexural building blocks and from the connected rigid body, as is done in typical finite element methods. Unlike previous

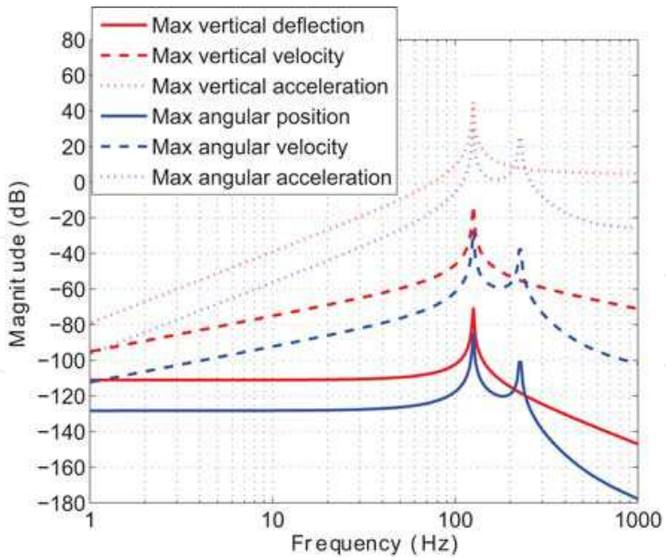


Fig. 7. The maximum amplification of states for an unit input vector (along any direction in the position space) is plotted for the case when a 1° misalignment of one of the flexural beam units is caused by a manufacturing error. Note that the system is now coupled as seen from the variation of the singular values.

works on flexure modeling, we found that Timoshenko beam bending models capture shear effects that dominate for short flexural beam lengths. We identified the key performance trade-offs in range, load-capacity, and natural frequencies of the first three modes of the diaphragm flexure. Redundancy in constraints was exploited to improve on load-capacity while ensuring the range or natural frequency requirements are met. Further, a control analysis based on singular value decomposition was formulated to capture the maximum values of performance variables such as linear or angular position and their derivatives. While perfect symmetry ensures decoupling between the modes, it was found that the amplification signature changes significantly in the presence of slight asymmetry caused by manufacturing errors. The dynamic modeling and state-space performance analysis detailed in this chapter are intended to serve as design tools for implementing high-precision motion control applications, and in particular, angular alignment based on diaphragm flexures.

## APPENDIX

### A.1 Distributed parameter model and approximation

The set of partial differential equations governing Timoshenko beam bending and St. Venant's torsion under the assumptions stated in Section 2.1 can be written in terms of the deflection $w(x,\ t)$, slope $\theta(x,\ t)$, and angle of twist $\phi(x,\ t)$ as follows [21, 20]:

$$EI_{yy}\frac{\partial^2\theta(x,t)}{\partial x^2}+\kappa AG\left\{\frac{\partial w(x,t)}{\partial x}-\theta(x,t)\right\} -\rho I_{yy}\frac{\partial^2\theta(x,t)}{\partial t^2}=0 \tag{14}$$

$$\rho A\frac{\partial^2 w(x,t)}{\partial x^2}-\kappa AG\left\{\frac{\partial^2 w(x,t)}{\partial x^2}-\frac{\partial\theta(x,t)}{\partial x}\right\}=0 \tag{15}$$

$$GJ_{xx}\frac{\partial^2\phi(x,t)}{\partial x^2}+I_{xx}\frac{\partial^2\phi(x,t)}{\partial t^2}=0 \tag{16}$$

where $\rho$, $E$, $GJ_{xx}$ are the density, elastic modulus, and torsional rigidity, respectively; $A$, $I_{yy}$, and $\kappa$ are the cross-sectional area, area moment of inertia about the neutral axis Y, and a geometry-dependent shear-factor, respectively. For a rectangular cross-section $\kappa$ assumes a value of 0.833 [25].

The component values of the mass **M** and stiffness **K** matrices are listed in Tables 4 and 5. The parameters used in the tables are $\alpha=\left\{\frac{1}{1+2p}\right\}^2$ and $\beta=\frac{EI_{yy}}{6}\frac{c^2}{l^5}$, where $p=(\frac{c}{\ell})^2$, and $c=\sqrt{\frac{6EI_{yy}}{\kappa AG}}$ representing the length scale at which effects of shear dominate. For a flexural beam with rectangular cross-section of height $H$, $c$ reduces to $\sqrt{1.1(1+\nu)}H$, where $\nu$ is the poisson's ratio of the material.

$$\begin{array}{lcl}
M_1 & = & \alpha m_f[\frac{13}{35}+\frac{7}{5}(\frac{c}{\ell})^2+\frac{4}{3}(\frac{c}{\ell})^4]+\frac{6}{5}\frac{\rho\alpha I_{yy}}{\ell}\\
M_2 & = & -\alpha m_f\ell[\frac{11}{210}+\frac{11}{60}(\frac{c}{\ell})^2+\frac{1}{6}(\frac{c}{\ell})^4]\\
 & & +\rho\alpha I_{yy}[\frac{1}{10}+(\frac{c}{\ell})^2]\\
M_3 & = & \alpha m_f\ell^2[\frac{1}{105}+\frac{1}{30}\{(\frac{c}{\ell})^2+(\frac{c}{\ell})^4\}]\\
 & & +\rho\alpha I_{yy}\ell[\frac{2}{15}+\frac{1}{3}(\frac{c}{\ell})^2+\frac{4}{3}(\frac{c}{\ell})^4]\\
M_4 & = & \frac{I_{xx}}{3}
\end{array}$$

Table 4. Mass matrix component values

$$\begin{array}{lcl}
K_1 & = & \alpha\frac{12EI}{\ell^3}+144\alpha\beta\\
K_2 & = & -\alpha\frac{6EI}{\ell^2}-72\alpha\beta\\
K_3 & = & \alpha\frac{4EI}{\ell}[1+(\frac{c}{l})^2+(\frac{c}{l})^4]+36\alpha\beta\\
K_4 & = & \frac{GJ_{xx}}{\ell}
\end{array}$$

Table 5. Stiffness matrix component values

### A.2 Decoupled arrangements

To identify the designs of diaphragm flexures that are close to being statically and dynamically decoupled, numerical methods can be used to solve the conditions given in Eq. (8). A geometric interpretation of the first two conditions of Eq. (8) is presented as:

$$\sum_{i=1}^{n}(cos\alpha_i+jsin\alpha_i)=0; \tag{17}$$

where $j$ is the imaginary number $\sqrt{-1}$. In the complex plane, the first two conditions of Eq. (8) hence represents a number $n$ of unit vectors radiating from the origin and adding up to zero. An easy guess of a subset $\Gamma_s$ of the solution space $\Gamma$ is possible if we consider the case when the flexures are symmetrically arranged around the central rigid mass. Some possible solutions present in the symmetry solution subset $\Gamma_s$ are as follows:

i. For odd values of $n$, $n \geq 3$, a possible solution subset is $\alpha_i=\varphi+\frac{(i-1)2\pi}{n}$ for $i$ = 1, 2, 3, … $n$ and $0 \leq \varphi < \frac{2\pi}{n}$.
ii. For even values of $n$, $n \geq 4$, there is an $\frac{n}{2}$ -fold symmetry, i.e. there are $\frac{n}{2}$ axes about which the flexural units are arranged symmetrically. A possible solution is one with all

unit vectors symmetrically arranged $\frac{2\pi}{n}$ apart, i.e. $\alpha_i = \varphi + \frac{(i-1)2\pi}{n}$ for $i$ = 1, 2, 3, …$n$ and $0 \leq \varphi < \frac{2\pi}{n}$. Another set can be obtained simply by rotating any two (or multiples of two) unit vectors adjacent to any axes of symmetry by the same angle, one in clockwise direction, and the other in counter-clockwise direction. This possible solution is illustrated in Fig. 8.

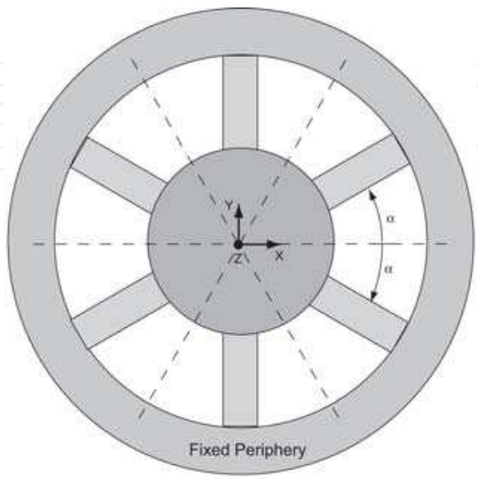


Fig. 8. A solution subset to the case when $n$ = 6, corresponding to three-fold symmetry with angle between any two constraints being $2\alpha = 60^{o}$. The dashed lines denote the axes of symmetry. If the flexure beams on either side of the horizontal axis of symmetry are brought symmetrically closer by an angle $\Delta\alpha$, they still satisfy the decoupling conditions of Eq. (8).

## 6. Acknowledgements

This work was supported by funding grants from the Manufacturing Systems and Technology program under the Singapore MIT Alliance. The first author would like to thank Ajay A. Deshpande and Mythili R. Vutukuru for their discussions on parts of the analysis.

## 7. References

[1] Loney GC, "High bandwidth steering mirror," US Patent 5,110,195, 1992.
[2] Choi BJ, Sreenivasan SV, Johnson S, et al, "Design of orientation stages for step and flash imprint lithography," Precision Engineering, Journal of the International Societies for Precision Engineering and Nanotechnology, vol. 25 (3), pp 192-199, July 2001.
[3] Choi KB, Lee JJ "Passive compliant wafer stage for single-step nano-imprint lithography,' Review of Scientific Instruments, 76 (7): Art. No. 075106 Jul 2005.
[4] Kendale AM, "Automation of soft lithographic microcontact printing," SM thesis, Department of Mechanical Engineering, Massachusetts Institute of Technology, Cambridge MA, 2002.
[5] Chan HB, Aksyuk VA, Kleiman RN, et al, "Quantum mechanical actuation of microelectromechanical systems by the Casimir force," Science, vol. 291 (5510): 1941-1944, Mar 2001.
[6] V. Shilpiekandula, "Progress through Mechanics: Small-scale Gaps," *Mechanics* (Publication of the American Academy of Mechanics), vol. 35, no. 9-10, pp. 3-6, Sep-Oct 2006.

[7] Slocum AH, "Precision machine design," Englewood Cliffs, NJ, Prentice Hall, 1992.
[8] Smith ST, "Flexures: elements of elastic mechanisms," Amsterdam, Gordon and Breach, 2000.
[9] Awtar S, Slocum AH, Sevincer E. "Characteristics of beam-based flexure modules," Journal of Mechanical Design, vol. 129 (6): 625-639 Jun 2007.
[10] V. Shilpiekandula and K. Youcef-Toumi, "Modeling and Control of a Programmable Filter for Separation of Biologically Active Molecules," In Proceedings of *American Control Conference*, pp. 394-399, June 2005.
[11] Awtar S and Slocum AH, "Design of Flexure Stages based on a Symmetric Diaphragm Flexure,' In Proceedings of American Society for Precision Engineering Annual Meeting, no. 1803, Norfolk, VA, 2005.
[12] Lobontiu N, "Compliant mechanisms: design of flexure hinges," Boca Raton, CRC Press, 2003; Howell LL, "Compliant mechanisms," New York , Wiley 2001.
[13] Jones RV, "Instruments and Experiences: Papers on Measurement and Instrument Design," John Wiley, 1988.
[14] Li Z, and S. Kota, "Dynamic Analysis of Compliant Mechanisms, "Proceedings of DETC, 27th Biannual Mechanisms and Robotics Conference," Sep 29 - Oct 2, Montreal, Canada, 2002.
[15] Choi KB, "Dynamics of a compliant mechanism based on flexure hinges," Proceedings of the Institution of Mechanical Engineers, Part-C, Journal of Mechanical Engineering Science 219 (2): 225-235 Feb 2005.
[16] Choi KB, Han CS, "Optimal design of a compliant mechanism with circular notch flexure hinges," Proceedings of the institution of Mechanical Engineers, Part-C, Journal of Mechanical Engineering Science 221 (3): 385-392 Mar 2007.
[17] Weaver W, Timoshenko SP, Young DH, "Vibration problems in engineering," New York, Wiley, 1990.
[18] Meirovitch L, "Computational Methods in Structural Dynamics," Sijthoff Noordhoff, Rockville MD, 1980.
[19] Dwivedy SK, Eberhard P. "Dynamic analysis of flexible manipulators, a literature review," Mechanism and Machine Theory, vol. 41 (7): 749-777, July 2006.
[20] Prezmieniecki JS, "Theory of matrix structural analysis," New York, McGraw-Hill, 1968.
[21] Ganesan N and Engels RC, "A dynamic finite element model for the Timoshenko beam," AIAA-1990-3547 Space Programs and Technologies Conference, Huntsville AL, Sep 1990.
[22] Inman DJ, "Engineering vibration," Englewood Cliffs, NJ, Prentice Hall,1994.
[23] Varanasi KK and Nayfeh SA, "Damping of Flexural Vibration Using Low-Density, Low-Wave-Speed Media," Journal of Sound and Vibration, vol. 292, pp. 402-414, 2006.
[24] Deo HV, Suh NP,"Mathematical transforms in design: Case study on feedback control of a customizable automotive suspension," CIRP Annals – Manufacturing Technology, vol. 53 (1), pp. 125-128, 2004.
[25] Hsu JC, Lee HL, Chang WJ, "Flexural vibration frequency of atomic force microscope cantilevers using the Timoshenko beam model," Nanotechnology, vol.18 (28): Art. No. 285503, July 2007.
[26] Varanasi KK, Nayfeh SA, "The Dynamics of Lead-Screw Drives: Low-Order Modeling and Experiments," Journal of Dynamic Systems, Measurement, and Control, Transactions of the ASME, vol. 126, pp. 388-396.
[27] Skogestad S and Postlethwaite I, "Multivariable feedback control: analysis and design," Hoboken, NJ, John Wiley, 2005.


**Motion Control**

Edited by Federico Casolo

ISBN 978-953-7619-55-8
Hard cover, 590 pages
**Publisher** InTech
**Published online** 01, January, 2010
**Published in print edition** January, 2010

The book reveals many different aspects of motion control and a wide multiplicity of approaches to the problem as well. Despite the number of examples, however, this volume is not meant to be exhaustive: it intends to offer some original insights for all researchers who will hopefully make their experience available for a forthcoming publication on the subject.

**How to reference**

In order to correctly reference this scholarly work, feel free to copy and paste the following:

Vijay Shilpiekandula and Kamal Youcef-Toumi (2010). Dynamic Modeling and Performance Trade-offs in Flexure-based Positioning and Alignment Systems, Motion Control, Federico Casolo (Ed.), ISBN: 978-953-7619-55-8, InTech, Available from: http://www.intechopen.com/books/motion-control/dynamic-modeling-and-performance-trade-offs-in-flexure-based-positioning-and-alignment-systems

INTECH
open science | open minds

**InTech Europe**
University Campus STeP Ri
Slavka Krautzeka 83/A
51000 Rijeka, Croatia
Phone: +385 (51) 770 447
Fax: +385 (51) 686 166
www.intechopen.com

**InTech China**
Unit 405, Office Block, Hotel Equatorial Shanghai
No.65, Yan An Road (West), Shanghai, 200040, China
中国上海市延安西路65号上海国际贵都大饭店办公楼405单元
Phone: +86-21-62489820
Fax: +86-21-62489821

IntechOpen